Hindawi Publishing Corporation
Shock and Vibration
Volume 2015, Article ID 426876, 13 pages
http://dx.doi.org/10.1155/2015/426876

Research Article

An Exact Analytical Solution to Exponentially Tapered Piezoelectric Energy Harvester

H. Salmani,[1] G. H. Rahimi,[2] and S. A. Hosseini Kordkheili[3]

[1]*Department of Aerospace Engineering, Tarbiat Modares University, Jalal Ale Ahmad Highway, P.O. Box 14115-111, Tehran, Iran*
[2]*Department of Mechanical Engineering, Tarbiat Modares University, Jalal Ale Ahmad Highway, P.O. Box 14115-111, Tehran, Iran*
[3]*Department of Aerospace Engineering, Sharif University of Technology, Azadi Street, P.O. Box 11365-11155, Tehran, Iran*

Correspondence should be addressed to G. H. Rahimi; rahimi_gh@modares.ac.ir

Received 26 January 2015; Accepted 20 April 2015

Academic Editor: Chao Tao

It has been proven that tapering the piezoelectric beam through its length optimizes the power extracted from vibration based energy harvesting. This phenomenon has been investigated by some researchers using semianalytical, finite element and experimental methods. In this paper, an exact analytical solution is presented to calculate the power generated from vibration of exponentially tapered unimorph and bimorph with series and parallel connections. The mass normalized mode shapes of the exponentially tapered piezoelectric beam with tip mass are implemented to transfer the proposed electromechanical coupled equations into modal coordinates. The steady states harmonic solution results are verified both numerically and experimentally. Results show that there exist values for tapering parameter and electric resistance in a way that the output power per mass of the energy harvester will be maximized. Moreover it is concluded that the electric resistance must be higher than a specified value for gaining more power by tapering the beam.

1. Introduction

The dream of making sensor network nodes to monitor mechanical systems' behavior is being achieved by applying low power, light weight, and self-sustained wireless sensors, which are capable of gaining required energy from environment. Converting light, thermal, and mechanical energies into electrical energy has been the most common methods to supply sensors' power. Electromagnetic, electrostatic, and piezoelectric transducers are three usual conversion methods of mechanical energy into electrical energy [1]. Electromagnetic convertors have been widely used in order to generate electricity out of mechanical energy since the early 1930s [2]. During the last decade, implementing piezoelectric materials in energy harvesting devices has been extensively investigated by researchers, because of their light weight, direct implementation, and wide range of frequencies applications. Piezoelectric energy harvester is usually constructed of piezoelectric layers attached to a substrate, and its fundamental frequency is adjusted by employing tuning mass, while it is mounted on a vibrating system.

As the highest performance of the piezoelectric energy harvesters occurs at their fundamental frequencies, at the early stage of the development of these devices, an equivalent single degree of freedom (SDOF) model is employed to estimate generated power [3, 4]. Later on, Erturk and Inman [5] improved SDOF model by adding separately treated strain rate and air damping terms and introducing a correction factor for varying tip mass to beam mass ratio. Although SDOF model gives a simple expression to study the energy harvester's behavior, it lacks several important aspects of the device such as dynamic mode shapes and accurate strain distribution. These lacks have been managed through introducing a correction factor for an improved lumped parameter model by Wang and Lu [6]. Knowing that SDOF model is a simple method to assess the harvester at a limited frequency range around the fundamental frequency of the beam, Sodano et al. [7] proposed a Rayleigh-Ritz method to calculate the power harvested from piezoelectric material including damping effect in higher modes. Erturk and Inman [8, 9] also employed eigenfunction expansion method using mass normalized mode shapes of unimorph and bimorph

beams with tip mass to solve the coupled electromechanical formulation of energy harvesting devices.

The need for more efficient devices has encouraged researchers to present electrical and mechanical solutions in order to increase the power generation of piezoelectric vibration based energy harvesters. The most common approach used to increase the performance of energy harvesters is their geometry modification, which creates uniform strain distribution through the beam's length. In this situation the electric charge is distributed uniformly and average power is higher than varying charge piezoelectric layer [10]. Baker et al. [11] observed that a triangular beam can harvest 50% more energy than the rectangular one, while the local overstrain occurrence is vanished by uniform strain distribution. Accepting the effects of uniform strain distribution on the harvested energy from the beam, researchers have started to examine the effects of different parameters on the harvester's performance either numerically [12–18] or analytically [19–23]. Although numerical methods are valuable for easy implementation as well as doing parameters study, such as geometry [13–17] and tip mass [12, 18], they are time consuming and do not lead to an exact solution for the problem. On the other hand, deriving analytical solution is an intricate or almost impossible task if the governing differential equation does not belong to those familiar ones with closed form solution.

Due to the existence of exact solution for eigenmodes of a uniform beam problem, a closed form expression can be obtained to present the harvester's behavior [8, 9]. However, solving trapezoidal beams dictates taking into account assumed modes as space dependent variables. Goldschmidtboeing and Woias [19] used rectangular beam eigenmodes to form mass, stiffness, coupling, and capacitance matrices of a triangular beam which were derived by Rayleigh-Ritz method. Dietl and Garcia [20] also applied admissible mode shapes of slender prismatic beam with tip mass to study the performance of a rectangular, linear taper and reverse taper energy harvester. Rosa and de Marqui Jr. [21] implemented Rayleigh-Ritz method and Euler-Bernoulli assumptions to investigate the behavior of linear and reverse tapered energy harvesters. The Differential Quadrature Method (DQM) is another way that was used to extract mode shapes of a beam with variable width in order to form the reduced order model of electromechanical equations [23]. In addition to tapering with just varying width, the piezoelectric energy harvesters can be also modified by changing the beam thickness [22].

According to this literature survey the approximated mode shapes have been employed to solve the nonuniform cross section piezoelectric energy harvesters' governing equations. In this paper, exact normalized mode shapes of exponential beam with tip mass [24] are utilized to convert the governing electromechanical equations into modal space to calculate the power generated from piezoelectric energy harvesters. The strain rate and air damping terms are also considered to define the damping effect more accurately. After verifying the proposed formulations numerically and experimentally, parametric study is performed on beam's length, tapering parameter, and electric resistance to investigate their effects on the energy harvesting device's performance. In this study, we have considered unimorph and bimorph with series connection as well as bimorph with parallel connection for all the cases.

2. Analytical Solution

2.1. Electromechanical Formulation. Piezoelectric energy harvester, as shown in Figure 1, is composed of a beam embedded by piezoelectric layers and is excited at its base. It is assumed that the piezoelectric layer is perfectly bonded to the substrate layer, while the integrated beam's width is varying exponentially through the length by $b(x) = b_0 e^{-cx}$, where c is tapering parameter. A proof mass is also attached on the tapered beam's tip to regulate the fundamental frequency.

Because of the low thickness of the beam, the Euler-Bernoulli assumptions are employed to develop the displacement field. The governing Equation of Motion (EoM) of a beam embedded by piezoelectric layer using Euler-Bernoulli assumptions is given as [8]

$$\frac{\partial^2 M(x,t)}{\partial x^2} + \frac{\partial^2}{\partial x^2}\left(C_s I(x)\frac{\partial^3 w(x,t)}{\partial x^2 \partial t}\right) + C_a \frac{\partial w(x,t)}{\partial t} + m(x)\frac{\partial^2 w(x,t)}{\partial t^2} = -\left[m(x) + M_t \delta(x-L)\right]\frac{\partial^2 w_b(x,t)}{\partial t^2} \tag{1}$$

in which C_s and C_a are equivalent strain rate and viscous air damping coefficients, respectively. w is the beam transverse deflection and w_b is the base excitation displacement along z direction, while $m(x)$ and M_t are mass per unit length and tip point mass, respectively. Area moment of inertia of the beam's cross section changes exponentially; that is, $I(x) = I_0 e^{-cx}$, in which I_0 is the moment of inertia of the beam at $x = 0$. The internal moment of the beam $M(x,t)$ is calculated by integrating the stress moment through the thickness as follows:

$$M(x,t) = -\int_{t_s} \sigma_s b(x)\, z\, dz - \int_{t_p} \sigma_p b(x)\, z\, dz. \tag{2}$$

In (2) σ_s and σ_p are defined as the normal stress in x direction at substrate and piezoelectric layers, respectively. Using the constitutive equation of isotropic and piezoelectric material, the normal stresses are formulated as

$$\begin{aligned} \sigma_s &= E_s \varepsilon_1^s(x,t) \\ \sigma_p &= E_p\left(\varepsilon_1^p(x,t) - d_{31}E_3(t)\right), \end{aligned} \tag{3}$$

where E_s and E_p are the modulus of elasticity of substrate and piezoelectric materials, respectively. Mechanical strain $\varepsilon_1(x,t) = -z(\partial^2 w(x,t)/\partial x^2)$ is calculated by applying the Euler-Bernoulli assumption. Piezoelectric electromechanical coupling is mathematically modeled by d_{31}, and $E_3(t) =$

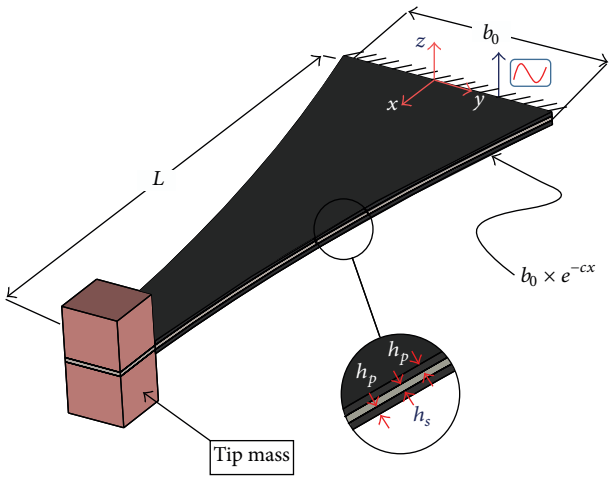

Figure 1: Piezoelectric energy harvester.

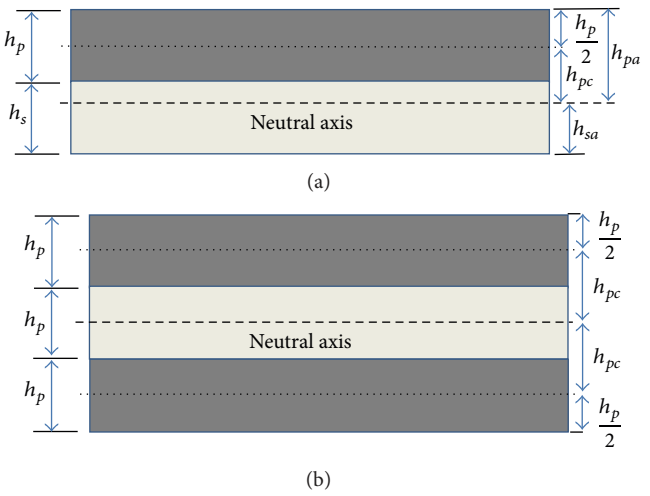

Figure 2: Piezoelectric beam cross section: (a) one-layered piezoelectric beam and (b) two-layered piezoelectric beam.

$-v(t)/h_p$ is the electric field through the z direction, where $v(t)$ is the generated piezoelectric voltage. Substituting (3) into (2) gives the internal bending moment as

$$M(x,t) = EI(x)\frac{\partial^2 w(x,t)}{\partial x^2} + \vartheta(x)\,v(t), \tag{4}$$

where $EI(x)$ is the flexural rigidity of the composite beam and is calculated as

$$EI(x) = b(x)\left[E_s\frac{h_s^3}{12} + 2\frac{E_p}{3}\left(\left(\frac{h_s}{2}+h_p\right)^3 - \frac{h_s^3}{8}\right)\right] \tag{5}$$

for a two-layered piezoelectric beam, and

$$EI(x) = b(x)\left[\frac{E_s\left(h_b^3 - h_a^3\right) + E_p\left(h_c^3 - h_b^3\right)}{3}\right] \tag{6}$$

for one-layered piezoelectric energy harvester. Geometrical parameters of (5) and (6) are shown in Figure 2.

In (6) h_a, h_b, and h_c are defined as

$$\begin{aligned} h_a &= -h_{sa};\\ h_b &= h_{pa} - h_p;\\ h_c &= h_{pa}, \end{aligned} \tag{7}$$

where h_{sa} is calculated as follows:

$$h_{sa} = \frac{h_p^2 + 2h_p h_s + \left(E_s/E_p\right)h_s^2}{2\left(h_p + \left(E_s/E_p\right)h_s\right)}. \tag{8}$$

Also $\vartheta(x)$ in (4) is an electromechanical coupling term of the bending moment, in which one-layered piezoelectric beam is calculated as

$$\vartheta(x) = -b(x)\frac{E_p d_{31}}{2h_p}\left(h_c^2 - h_b^2\right) \tag{9}$$

and for two-layered piezoelectric beam, its value depends on the types of electrical connection and is derived as follows:

$$\begin{aligned} \vartheta_p(x) &= 2\vartheta_s(x)\\ &= b(x)\frac{E_p d_{31}}{h_p}\left[\left(\frac{h_s^2}{4}\right) - \left(h_p + \frac{h_s}{2}\right)^2\right], \end{aligned} \tag{10}$$

where subscripts "s" and "p" indicate series or parallel connections, respectively. These two types of electrical connections are indicated in Figure 3.

Substituting (4) into (1) and considering the location of the piezoelectric layer along the x direction using Heaviside function $\mathrm{He}(x)$ gives the governing EoM in terms of $w(x,t)$ and $v(t)$ as

$$\begin{aligned} &\frac{\partial^2}{\partial x^2}\left[EI(x)\frac{\partial^2 w(x,t)}{\partial x^2}\right] + \frac{\partial^2}{\partial x^2}\left[C_s I(x)\frac{\partial^3 w(x,t)}{\partial x^2 \partial t}\right]\\ &\quad + C_a\frac{\partial w(x,t)}{\partial t} + m(x)\frac{\partial^2 w(x,t)}{\partial t^2}\\ &\quad + \frac{\partial^2}{\partial x^2}\left[\vartheta(x)\,v(t)\left[\mathrm{He}(x) - \mathrm{He}(x-L)\right]\right]\\ &= -\left[m(x) + M_t\delta(x-L)\right]\frac{\partial^2 w_b(x,t)}{\partial t^2}. \end{aligned} \tag{11}$$

One more necessary equation to determine unknowns $w(x,t)$ and $v(t)$ is derived out of the second constitutive equation of piezoelectric material; that is,

$$D_3(x,t) = d_{31}\sigma_p(x,t) + \varepsilon_{33}^T E_3(t), \tag{12}$$

where D_3 is the electric displacement and ε_{33}^T is the permittivity at constant stress. Rewriting (12) in terms of $w(x,t)$ and $v(t)$ gives

$$D_3(x,t) = -d_{31}E_p h_{pc}\frac{\partial^2 w(x,t)}{\partial x^2} - \varepsilon_{33}^s\frac{v(t)}{h_p}, \tag{13}$$

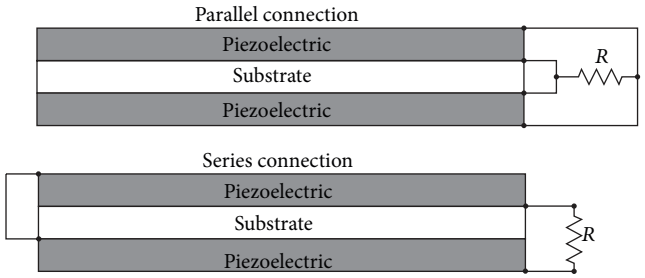

Figure 3: Parallel and series electrical connections.

where ε_{33}^{s} is the permittivity at constant strain. The electric charge generated at piezoelectric layer is calculated by applying the electric displacement as follows:

$$\begin{aligned} q(t) &= \int_S D_3 \cdot n\, dA \\ &= -\int_0^L b(x)\left(d_{31}E_p h_{pc}\frac{\partial^2 w(x,t)}{\partial x^2} + \varepsilon_{33}^{s}\frac{v(t)}{h_p}\right)dx, \end{aligned} \tag{14}$$

where n is the unit normal vector to the piezoelectric plane. The voltage of the piezoelectric layer is calculated after multiplying electric resistance R by electric current, which is the first derivative of electric charge with respect to time as

$$\begin{aligned} v(t) = Ri(t) &= R\frac{dq(t)}{dt} \\ &= -R\left(\int_0^L b(x)\, d_{31}E_p h_{pc}\frac{\partial^3 w(x,t)}{\partial x^2 \partial t}dx + \frac{\varepsilon_{33}^{s}}{h_p}\right. \\ &\left.\cdot \int_0^L b(x)\, dx\frac{dv(t)}{dt}\right). \end{aligned} \tag{15}$$

Equation (15) gives the voltage for a one-layered piezoelectric energy harvester, while the general form of the governing equation is given as

$$\begin{aligned} \alpha\frac{v(t)}{R} + \beta\frac{\varepsilon_{33}^{s}}{h_p}\int_0^L b(x)\, dx\frac{dv(t)}{dt} \\ = -\int_0^L b(x)\, d_{31}E_p h_{pc}\frac{\partial^3 w(x,t)}{\partial x^2 \partial t}dx, \end{aligned} \tag{16}$$

where

for one-layered piezoelectric beam $\alpha = \beta = 1$

for two-layered piezoelectric beam, parallel connection

$$\alpha = \frac{1}{2};\ \beta = 1 \tag{17}$$

for two-layered piezoelectric beam, series connection

$$\alpha = 1;\ \beta = \frac{1}{2}.$$

Equations (11) and (16) are two coupled governing differential equations of a variable width piezoelectric beam, which can be solved by implementing eigenfunction expansion method as

$$w(x,t) = \sum_{s=1}^{\infty}\varphi_s(x)\,\eta_s(t) \tag{18}$$

in which $\varphi_s(x)$ are mass normalized mode shapes of the beam and $\eta_s(t)$ are the modal coordinate.

2.2. Free Vibration of the Piezoelectric Exponentially Tapered Beam. As it was noted, in order to solve the coupled electromechanical equations, extracting the normalized eigenfunctions of the exponentially tapered beam is needed. The eigenfunctions are calculated by solving free vibration of the beam with clamped-free boundary conditions. The free vibration differential equation of a variable cross section beam by Euler-Bernoulli assumption is given as [24]

$$\frac{\partial^2}{\partial x^2}\left(EI(x)\frac{\partial^2 w(x,t)}{\partial x^2}\right) + m(x)\frac{\partial^2 w(x,t)}{\partial t^2} = 0. \tag{19}$$

For exponentially tapered beams, flexural rigidity and mass per unit length of the beam are exponentially varied along the x direction and are formulated as follows:

$$\begin{aligned} EI(x) &= EI_0 e^{-cx}; \\ m(x) &= m_0 e^{-cx}, \end{aligned} \tag{20}$$

where EI_0 and m_0 are the flexural rigidity and mass per unit length of the beam at $x = 0$. Using the method of separation of variables, that is, considering $(x,t) = \psi(x)T(t)$, the differential equation (19) is separated into spatial and temporal equations as follows:

$$\begin{aligned} \frac{d^2}{dx^2}\left(EI(x)\frac{d^2\psi(x)}{dx^2}\right) - \omega^2 m(x)\psi(x) = 0, \\ \ddot{T}(t) + \omega^2 T(t) = 0, \end{aligned} \tag{21}$$

where solution of the spatial differential equation leads to the eigenfunctions as follows:

$$\begin{aligned} \psi(x) &= e^{c(x/2)}\left[C_1\cosh(\xi x) + C_2\sinh(\xi x)\right. \\ &\left. + C_3\cos(\lambda x) + C_4\sin(\lambda x)\right];\quad \kappa > \frac{c^2}{4}, \\ \psi(x) &= e^{c(x/2)}\left[C_1\cosh\left(\frac{cx}{\sqrt{2}}\right) + C_2\sinh\left(\frac{cx}{\sqrt{2}}\right)\right. \\ &\left. + C_3 + C_4 x\right];\quad \kappa = \frac{c^2}{4}, \\ \psi(x) &= e^{c(x/2)}\left[C_1\cosh(\xi x) + C_2\sinh(\xi x)\right. \\ &\left. + C_3\cosh(\gamma x) + C_4\sinh(\gamma x)\right];\quad \kappa > \frac{c^2}{4} \end{aligned} \tag{22}$$

in which $\kappa^2 = \omega^2 m_0/EI_0$ and ξ, λ, and γ are given as

$$\xi = \frac{\sqrt{4\kappa + c^2}}{2},$$
$$\lambda = \frac{\sqrt{4\kappa - c^2}}{2}, \quad (23)$$
$$\gamma = \frac{\sqrt{c^2 - 4\kappa}}{2}.$$

In order to find the coefficients from C_1 to C_4, following boundary conditions of a clamped-free beam with a tip mass are employed:

$$\psi(x) = 0,$$
$$\left.\frac{d\psi(x)}{dx}\right|_{x=0} = 0,$$
$$\left\{\frac{d}{dx}\left[EI(x)\frac{d^2\psi(x)}{dx^2}\right] + \omega^2 M_t \psi(x)\right\}\Bigg|_{x=L} = 0, \quad (24)$$
$$\left[EI(x)\frac{d^2\psi(x)}{dx^2} - I_t\omega^2\frac{d\psi(x)}{dx}\right]\Bigg|_{x=L} = 0,$$

where I_t is the rotatory inertia of the tip mass. Nontrivial solution of this system of equations is available when the determinant of coefficient matrix equals zero. Solving the characteristic equation derived from the determinant gives the eigenvalues of the system and as a result the mode shapes of the system are specified. Mass normalized mode shapes of the beam are calculated using the following formulations [9]:

$$\phi_i(x) = \frac{\psi_i(x)}{\sqrt{\int_0^L \psi_i(x)\, m(x)\, \psi_i(x)\, dx + \psi_i(L)\, M_t \psi_i(L) + \left[\left(d\psi_i(x)/dx\right) I_t \left(d\psi_i(x)/dx\right)\right]\big|_{x=L}}}. \quad (25)$$

The orthogonality condition of the mass normalized modes shapes is given as follows [25]:

$$\int_0^L \phi_r(x)\, m(x)\, \phi_s(x)\, dx + \phi_r(L)\, M_t \phi_s(L) + \left[\frac{d\phi_r(x)}{dx} I_t \frac{d\phi_s(x)}{dx}\right]\Bigg|_{x=L} = \delta_{rs}, \quad (26)$$
$$\int_0^L \frac{d^2\phi_r(x)}{dx^2} EI(x) \frac{d^2\phi_s(x)}{dx^2} = \omega_r^2 \delta_{rs}$$

which can be used to transfer EoM to modal space.

2.3. Harmonic Base Excitation Solution. The mass normalized mode shapes of (25) are applied in eigenfunction expansion series of (18). Substituting (18) into coupled electromechanical equation (11) gives

$$\sum_{s=1}^{\infty} \frac{d^2}{dx^2}\left[EI(x)\frac{d^2\phi_s(x)}{dx^2}\right]\eta_s(t) + \sum_{s=1}^{\infty}\left\{\frac{d^2}{dx^2}\left[C_s I(x)\frac{d^2\phi_s(x)}{dx^2}\right] + C_a\right\}\frac{d\eta_s(t)}{dt} + m(x)\sum_{s=1}^{\infty}\phi_s(x)\frac{d^2\eta_s(t)}{dt^2} + \frac{d^2}{dx^2}\left[\vartheta(x)\left[\mathrm{He}(x) - \mathrm{He}(x-L)\right]\right] v(t) = -\left[m(x) + M_t\delta(x-L)\right]\frac{\partial^2 w_b(x,t)}{\partial t^2}. \quad (27)$$

Integrating (27) over the length of the beam after multiplying it by $\varphi_r(x)$ gives the EoM in modal space as follows:

$$\ddot{\eta}_r(t) + 2\zeta_r\omega_r\dot{\eta}_r(t) + \omega_r^2\eta_r(t) + \chi_r v(t) = f_r(t) \quad (28)$$

in which ω_r and ζ_r are natural frequency and damping ratio of the rth mode and χ_r and $f_r(t)$ are given as

$$\chi_r = \int_0^L \phi_r(x)\,\vartheta''(x)\,dx + \left.\frac{d\left(\phi_r(x)\,\vartheta(x)\right)}{dx}\right|_{x=0} - \left.\frac{d\left(\phi_r(x)\,\vartheta(x)\right)}{dx}\right|_{x=L} + 2\left(\phi_r(0)\,\vartheta'(0) - \phi_r(L)\,\vartheta'(L)\right), \quad (29)$$
$$f_r(t) = -\left[\int_0^L \phi_r(x)\, m(x)\, dx + M_t\phi_r(L)\right]\frac{d^2 g(t)}{dt^2}.$$

In order to change the partial differential equation (16) into ordinary differential equation with respect to time, (18) is also substituted into (16) as follows:

$$v(t) + R\frac{\beta}{\alpha}\left[\frac{\varepsilon_{33}^s}{h_p}\int_0^L b(x)\,dx\right]\frac{dv(t)}{dt} = -\sum_{r=1}^{\infty}\frac{Rd_{31}E_p h_{pc}}{\alpha}\int_0^L b(x)\frac{d^2\phi_r(x)}{dx^2}dx\dot{\eta}_r(t). \quad (30)$$

Simplifying (30) gives the second coupled ordinary differential equation of piezoelectric energy harvester as

$$\dot{v}(t) + \frac{1}{\tau_c}v(t) = \sum_{r=1}^{\infty}\varphi_r\dot{\eta}_r(t) \quad (31)$$

in which

$$\tau_c = R\frac{\beta}{\alpha}\left[\frac{\varepsilon_{33}^s}{h_p}\int_0^L b(x)\,dx\right],$$
$$\varphi_r = -\frac{d_{31}E_p h_{pc} h_p}{\beta\varepsilon_{33}^s}\frac{\int_0^L b(x)\,\phi_r''(x)\,dx}{\int_0^L b(x)\,dx}. \quad (32)$$

Here to find the harmonic solution of the exponentially tapered piezoelectric energy harvester, it is assumed that the base is moving harmonically in z direction, which means that

$$g(t) = Y_0 e^{j\omega t}. \quad (33)$$

Due to the harmonic excitation of the beam, the unknown terms $v(t)$ and $\eta_r(t)$ are also expected to be harmonic as follows:

$$v(t) = V_0 e^{j\omega t},$$
$$\eta_r(t) = H_r e^{j\omega t}. \quad (34)$$

The voltage amplitude V_0 is calculated by substituting (33) and (34) into (28) and (31) as

$$V_0 = \frac{j\omega\sum_{r=1}^{\infty}\left(\varphi_r F_r/\left(\omega_r^2 - \omega^2 + 2j\zeta_r\omega_r\omega\right)\right)}{\left(\left(1 + j\omega\tau_c\right)/\tau_c\right) + j\omega\sum_{r=1}^{\infty}\left(\varphi_r\chi_r/\left(\omega_r^2 - \omega^2 + 2j\zeta_r\omega_r\omega\right)\right)}, \quad (35)$$

where

$$F_r = Y_0\omega^2\left[\int_0^L \phi_r(x)\,m(x)\,dx + M_t\phi_r(L)\right] \quad (36)$$

and the temporal term amplitude H_r is given as

$$H_r = \frac{F_r - \chi_r V_0}{\omega_r^2 - \omega^2 + 2j\zeta_r\omega_r\omega}. \quad (37)$$

3. Results and Discussion

Using the analytical formulation of the exponentially tapered piezoelectric energy harvester discussed in this paper, some sample problems are solved to show the performance of the solution. Regarding lack of results on exponentially tapered piezoelectric beam in the literature, to verify the analytical solution a constant cross section piezoelectric beam is firstly considered and the results are compared with those from experimental and numerical methods as well as with those available in the literature for this case.

3.1. Experimental Verification of the Solution. As discussed previously, in this part a constant cross section beam (with $c = 0$) is tested using the experimental set up of Figure 4. Experimental test is conducted on a cantilever unimorph piezoelectric beam with a PZT4 patch of length $L = 60$ mm, width $b_0 = 10$ mm, and thickness $h_p = 0.6$ mm which is bonded to a steel beam with the same dimension but thickness $h_s = 0.7$ mm (Table 1). A tip of 18 grams of mass which contains 9-gram steel mass together with 9-gram accelerometer is attached to the free end of the beam as shown in Figure 4(a). This accelerometer measures the beam's response during experiment. The finite element model is created to be the same as the experimental model, while two steel cubes of $10 \times 10 \times 11.2$ mm^3 play the role of tip masses.

Table 1: PZT and steel material properties.

Material	Property	Value
PZT 4	C_{11} (GPa)	139
	C_{12} (GPa)	77.84
	C_{13} (GPa)	74.28
	C_{33} (GPa)	114.41
	C_{44} (GPa)	25.64
	C_{55} (GPa)	30.58
	e_{31} (Cm^{-2})	−5.2028
	e_{33} (Cm^{-2})	15.0804
	e_{15} (Cm^{-2})	12.7179
	ε_0 (Fm^{-1})	8.854×10^{-12}
	$\varepsilon_{11}/\varepsilon_0$	1475
	$\varepsilon_{22}/\varepsilon_0$	1475
	$\varepsilon_{33}/\varepsilon_0$	1300
	ρ (Kg/m^3)	7960
Steel	E (GPa)	200
	υ	0.3
	ρ (Kg/m^3)	7800

A 440 N Tira TV51144 shaker is then used to excite the test structure. During the test execution another accelerometer is also installed on the support to measure the applying acceleration. The output of the piezoelectric layer is connected to a NI USB4431 data acquisition system through a 100 Ω electric resistance. Figure 4(b) shows the schematic of the experimental setup.

As the modal parameters of the complex beam are required to do further analysis, an Operational Modal Analysis (OMA) is initially performed while the piezoelectric electrodes are short circuit. After this initial experiment the first natural frequency and the associated damping ratio are measured as 47.6 Hz and 4.9%, respectively. These modeling parameters are gathered in Table 2 for future citation. Then a sine sweep excitation from 10 to 100 Hz for duration of 20 seconds is applied on the piezoelectric energy harvester with 100 Ω electric resistance to examine the output voltage in the specified frequency range. Cancelling the noises is performed by averaging the results between 10 times repetition of the experiment.

Figure 5 depicts the voltage per the base acceleration versus frequency of the piezoelectric beam. This figure also compares the experimental results with the results from the finite element method of ANSYS, the presented analytical solution, and those from relations reported by Erturk and Inman [8, 9]. It reveals that the results from the present analytical solution are comparable with those from the experiments and the relations reported in [8, 9]. Analytically, in this situation $b(x)$ equals b_0, which means (10), (11), and

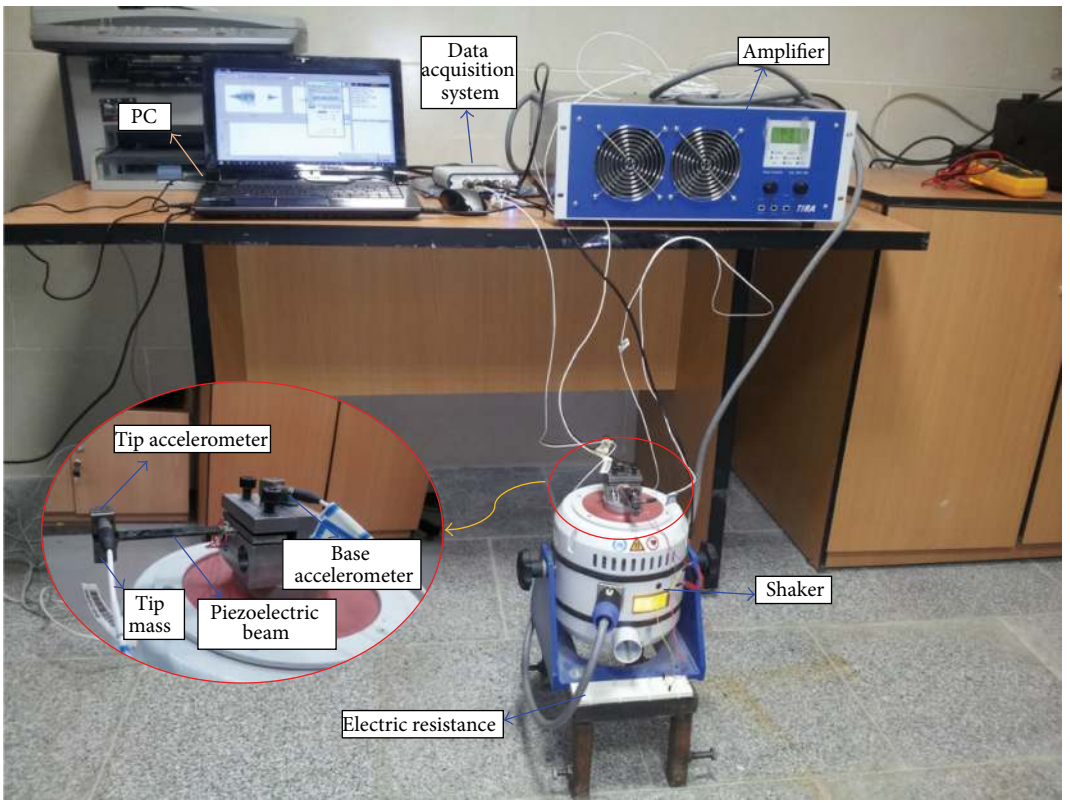

(a)

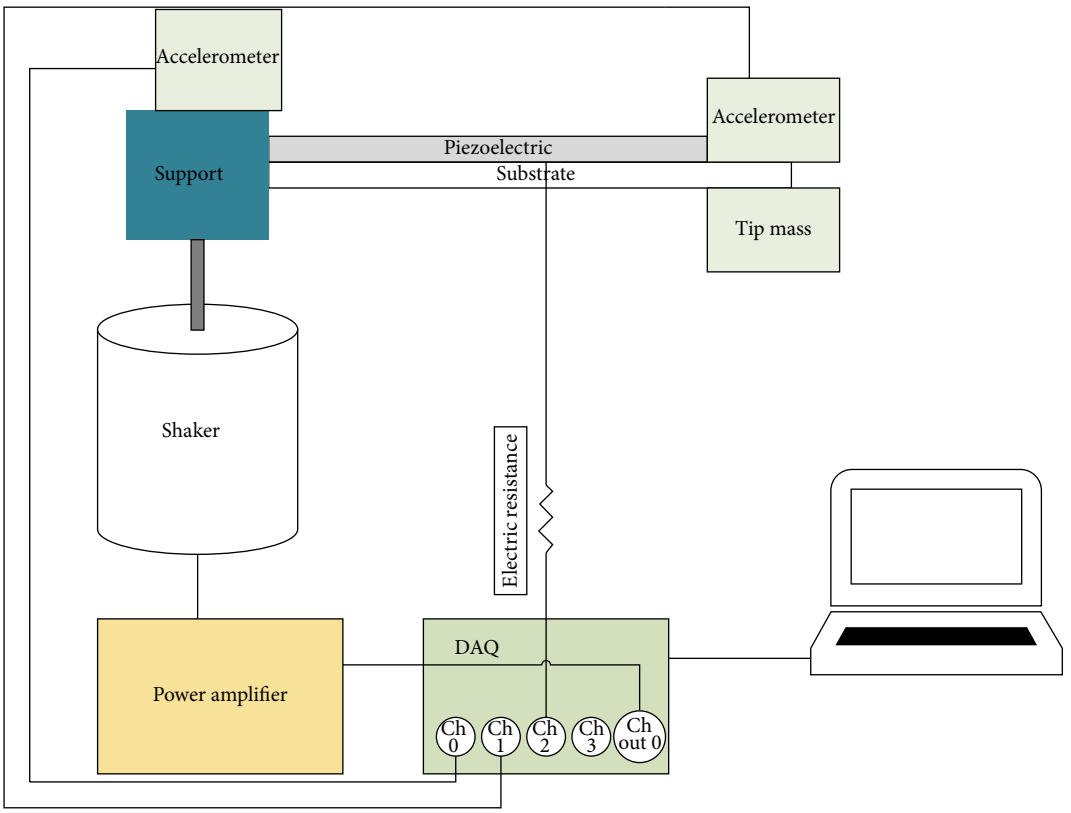

(b)

Figure 4: (a) Experiment equipment setup and (b) schematic of the experimental setup.

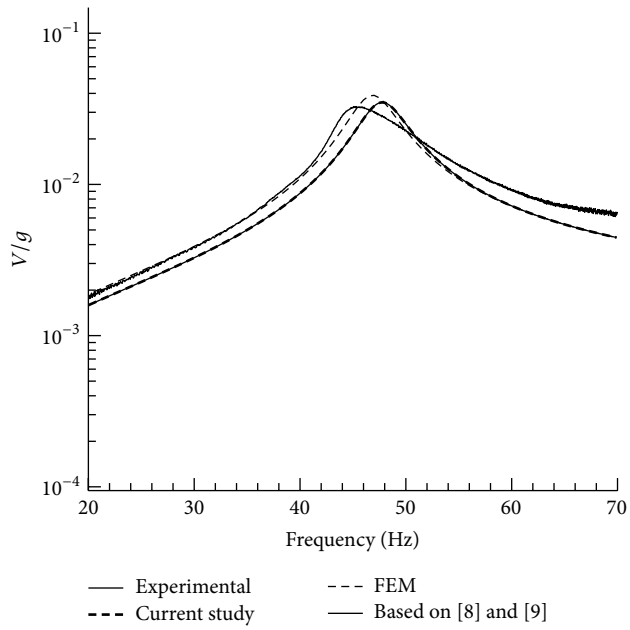

Figure 5: Output voltage/input acceleration versus frequency.

Table 2: Energy harvesters modelling parameters.

Parameter	Value
L (mm)	60
b_0 (mm)	10
h_s (mm)	0.7
h_p (mm)	0.6
M_t (gr)	9
z	0.049
R_l	100

(16) converge to those for unimorph energy harvester in [8], while the terms of tip mass are added from [9]. The simplified forms of (10), (11), and (16) for the case $c = 0$ are derived as follows:

$$\vartheta(x) = \vartheta = -\frac{b_0 E_p d_{31}}{2h_p}\left(h_c^2 - h_b^2\right),$$

$$\begin{aligned} &EI_0\frac{\partial^4 w(x,t)}{\partial x^4} + C_s I_0\frac{\partial^5 w(x,t)}{\partial x^4 \partial t} + C_a\frac{\partial w(x,t)}{\partial t} \\ &\quad + m_0\frac{\partial^2 w(x,t)}{\partial t^2} + \vartheta v(t)\left[\frac{d\delta(x)}{dx} - \frac{d\delta(x-L)}{dx}\right] \\ &\quad = -\left[m_0 + M_t\delta(x-L)\right]\frac{\partial^2 w_b(x,t)}{\partial t^2}, \\ &\frac{v(t)}{R} + \frac{\varepsilon_{33}^s b_0 L}{h_p}\frac{dv(t)}{dt} \\ &\quad = -\int_0^L b_0 d_{31} E_p h_{pc}\frac{\partial^3 w(x,t)}{\partial x^2 \partial t}dx. \end{aligned} \tag{38}$$

In accordance with Figure 5, it can be also concluded that the results of present work are in a good agreement with those from finite element solution of commercial software for analyzing piezoelectric beams, while the present study has lower computational effort and complexity.

3.2. Case Studies. Figure 6 plots geometry of the beam with different tapering parameter values (i.e., $c = 0$, 5, 10, 15, and 20). Although, increasing tapering parameter may lead to higher voltage to weight ratio [13], it also causes increasing fundamental frequency of the beam. In view of taking full advantage of beam to harvest energy, according to Figure 5, a designer needs to keep the first natural frequency of the beam close to the exciting frequency. For this purpose the designer can either use a thinner substrate layer or mount a tip mass. Some case studies are performed in this section to show the abilities of the presented analytical solution as a design tool to investigate the output voltage per unit mass of the energy harvester device. All geometrical parameters of the case studies are similar to those listed in Table 2, unless mentioned.

3.2.1. Numerical Verification of the Solution. Before going into the parameter study to refine the confidence, the results from the presented analytical solution are also verified for the beams with various tapering parameter as well as different types of electrical connections using finite element method. In this example, the electrical resistance is taken to be 1000 Ω, and the damping ratio is assumed to be 1 percent. Moreover, no tip mass is attached to the beam. For this verification procedure, the output voltage generated out of the piezoelectric beam at its fundamental frequency is tabulated in Table 3 for different tapering parameter and electrical connections. According to this table the maximum difference of these two methods is 3.6%, which means that the current formulation well predicts the tapered piezoelectric energy harvester's behavior. Also it can be noted that increasing tapering parameter may reduce the generated voltage per exciting acceleration, but at the same time it makes the structure lighter. Hence, if the total mass is an important design parameter, comparing the voltage per unit mass parameter for energy harvesters will be a real parameter during case studies. According to this statement we consider this parameter during our later studies.

3.2.2. Tapering Parameter Effects on Output Voltage

(a) Tuning the Natural Frequency Using Substrate Thickness. As we mentioned earlier, in order to take full advantage of beam to harvest energy, one needs to keep the first natural frequency of the beam close to the exciting frequency while tapering parameter is improved. In this section, tuning this natural frequency is done by changing substrate thickness for different length to width ratio. All parameters of the beam are the same as those in Section 3.2.1 for case $c = 0$. Figures 7–9 depict the voltage density ($V/m_{T0}g$) different tapering parameter taken at fundamental frequency for unimorph and bimorph with series and parallel connections. In these figures m_{T0} is defined as the total mass of the energy harvester.

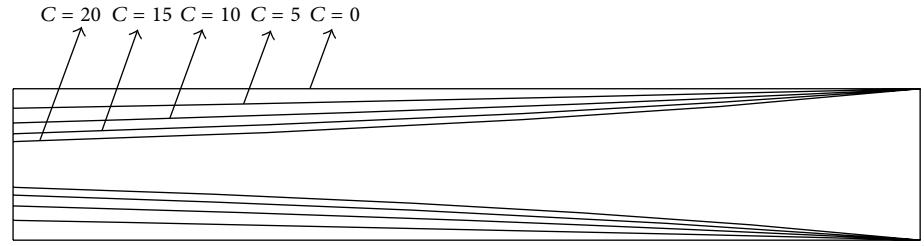

Figure 6: Geometry of the beam with different tapering parameter values.

Table 3: Comparison of analytic and FEM results.

C	0	5	10	15	20
Unimorph					
Analytic (V/g)	0.5711	0.499	0.438	0.3842	0.3377
FEM (V/g)	0.592561	0.516427	0.451596	0.395634	0.347023
Difference (%)	3.621737	3.374533	3.010656	2.890045	2.686565
Bimorph series					
Analytic (V/g)	0.6252	0.5479	0.4802	0.4214	0.3704
FEM (V/g)	0.64757	0.563801	0.490386	0.430593	0.377891
Difference (%)	3.454453	2.820321	2.077139	2.134963	1.982318
Bimorph parallel					
Analytic (V/g)	1.156	1.011	0.8847	0.7751	0.6805
FEM (V/g)	1.18912	1.03459	0.901908	0.788796	0.691405
Difference (%)	2.785253	2.28013	1.907955	1.736317	1.577223

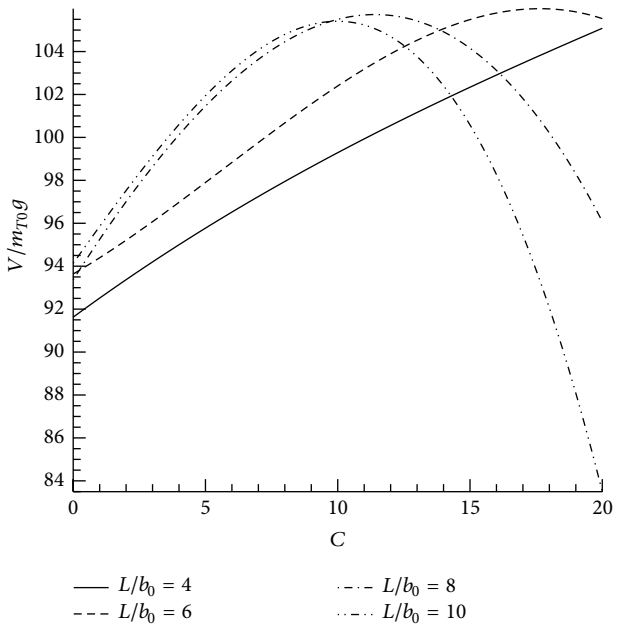

Figure 7: Tapering and length effects on unimorph modified thickness.

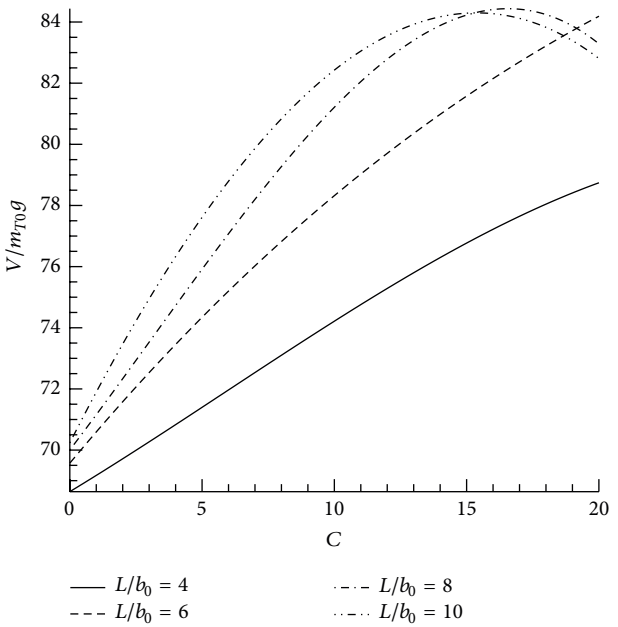

Figure 8: Tapering and length effects on bimorph with series connection, modified thickness.

Evaluating the results shows that tapering the beam with exponential distribution leads to extracting higher voltage density from the energy harvester. Moreover, tapering the beam makes a uniform strain distribution over the piezoelectric layer that causes more voltage generation [13]. For all cases, with increasing the beam's length to base width ratio,

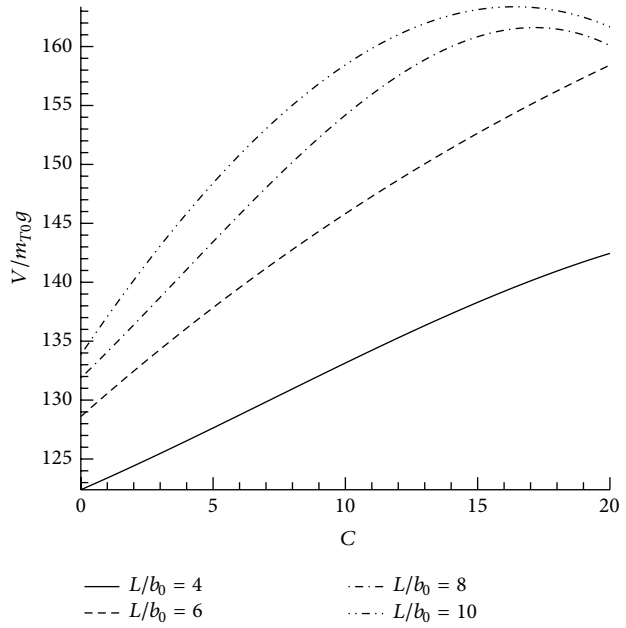

Figure 9: Tapering and length effects on bimorph with parallel connection, modified thickness.

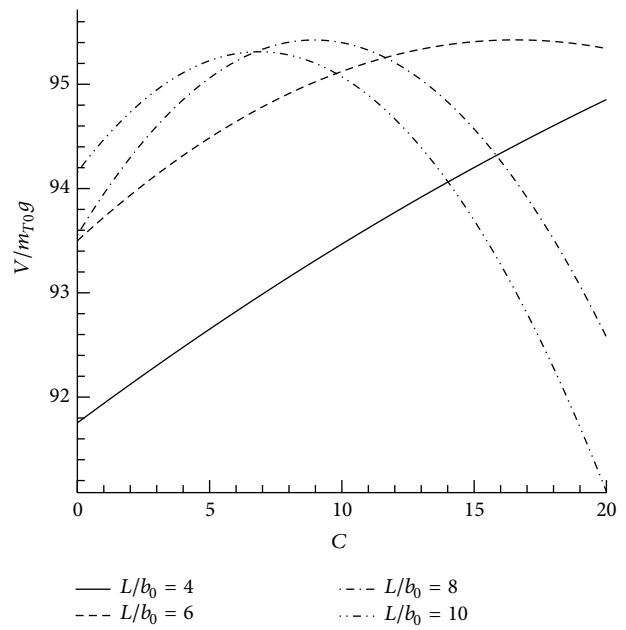

Figure 10: Tapering and length effects on unimorph, with tip mass.

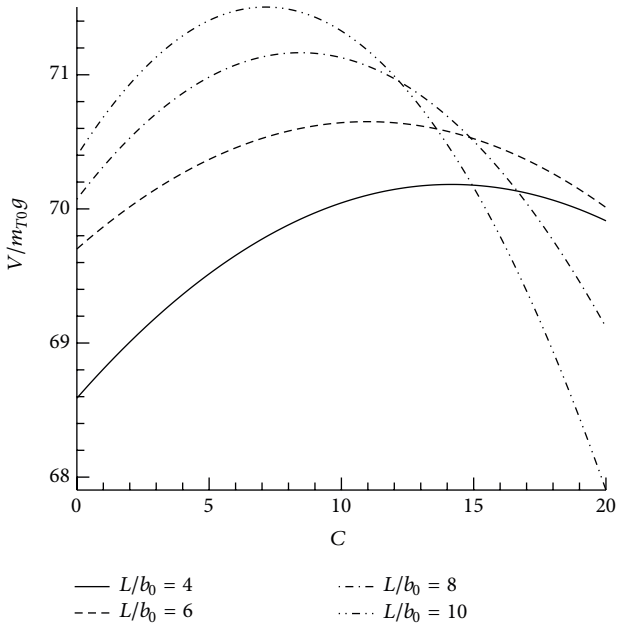

Figure 11: Tapering and length effects on bimorph with series connection, with tip mass.

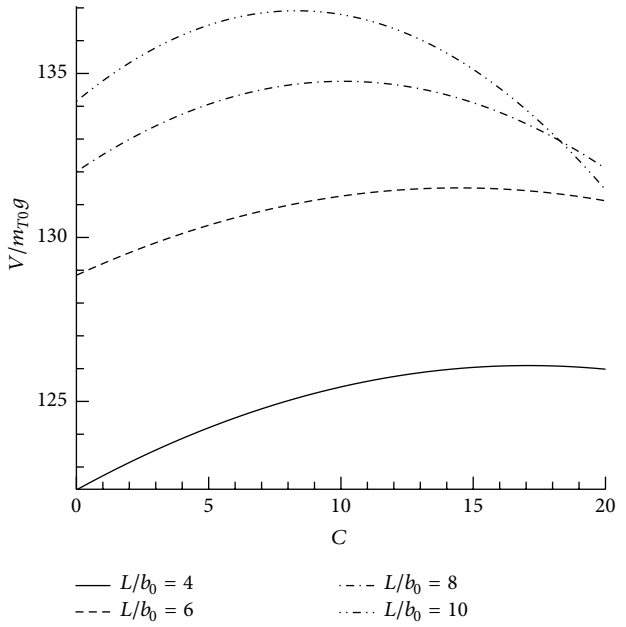

Figure 12: Tapering and length effects on bimorph with parallel connection, with tip mass.

the tapering parameter with the highest voltage density is decreased. It is also observed that increasing the beam's length causes increasing the voltage density, because of contributing more piezoelectric bulk during power generation.

(b) Tuning the Natural Frequency Using Tip Mass. Another way to adjust the first natural frequency of a beam with different tapering parameter is to add a tip mass. The results of the current models are plotted in Figures 10–12 for unimorph and bimorph with series and parallel connections.

According to these figures, the energy harvesting device with tip mass and varying tapering parameter behaves in a way similar to that of the beam without tip mass and varying thickness (i.e., Section 3.2.2 (a)). It means that by adding a tip mass designer would be also able to improve the voltage

density value for a beam. In this approach a mass is added to the system which makes the device weightier, and on the other hand tapering decreases beam's mass. Therefore, in this method the total mass of the system decreases in a lower rate in comparison with the previous method. Referring to (35) it can be noted that, for higher tapering parameters which are associated with weightier tip mass, the output voltage value improves. Compromising these effects may be the reason for achieving the maximum voltage density at the lower c in comparison with the previous method. In addition, comparing both tuning methods reveals that adding the tip mass decreases the value of voltage density of the beams with the same value of tapering parameter. Therefore, if the designed beam is strong enough to tolerate the stresses during its estimated life time, it is more appropriate to thin the substrate layer in order to tune its fundamental frequency otherwise adding the tip mass will be carried out, alternatively.

3.2.3. Tapering Parameter and Electric Resistance Effects on Output Power. Electric resistance is a critical parameter for extracting the maximum power density (P/mg^2) from the device [8]. In this section the same beam with $L = 80$ mm is considered and the substrate layer's thickness is changed to obtain a constant natural frequency for different c values. The power density versus electric resistance is depicted in Figures 13–15 for unimorph and bimorph with series and parallel connections. From these figures it is observed that there exists an optimum value of electric resistance which results in maximum power density for an energy harvesting device. This optimum value depends on tapering parameter. Increasing tapering parameter value leads to an increase in the optimum electric resistance. In addition, when electric resistance is smaller than a specified value, tapering would decrease the power density of the device, which is not desired. But for higher electric resistances, tapering parameter plays a key role for gaining maximum power with minimum weight. This value of the electric resistance and the amount of improvement in power density by tapering depends on the type of electric connection. In this example, for the highest value of the electric resistance, that is, 1 MΩ, exponential tapering will grow the power per mass of the device about 29 percent for unimorph and 14 and 52 percent for bimorph with series and parallel connections, respectively.

3.3. Exponentially Tapered versus Trapezoidal Energy Harvesters. Figure 16 depicts the considered geometries for exponentially and linearly tapered energy harvesters with the parameters in Table 4 which are the same as those employed by Rosa and de Marqui Jr. [21]. In presence of 1 KΩ and 1 MΩ electric resistances, both problems are solved and the results are compared with those reported by Rosa and de Marqui Jr. [21] in Figure 17. From this figure one can observe that because of its lower piezoelectric volume the voltage generated from exponentially tapered beam is lower than those from linearly tapered beam. However, the linearly tapered beam may produce lower voltage density. Therefore, a trade-off between voltage, weight, electric resistance, and ease of construction should be always carried out to lead to a better harvester.

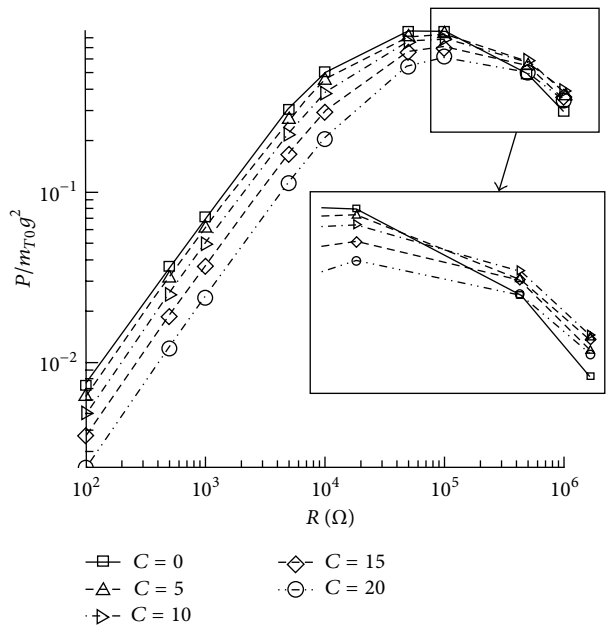

Figure 13: Tapering and electric resistance effects on unimorph.

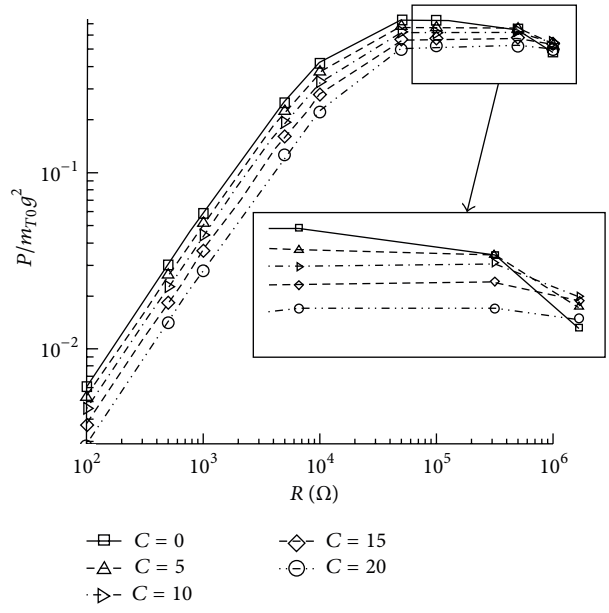

Figure 14: Tapering and electric resistance effects on bimorph with series connection.

4. Conclusions

In this paper, an analytical solution for exponentially tapered energy harvesting device has been presented. The proposed formulations can calculate the output voltage of unimorph and bimorph with series and bimorph with parallel connections, while the tip mass is also considered. Comparing the

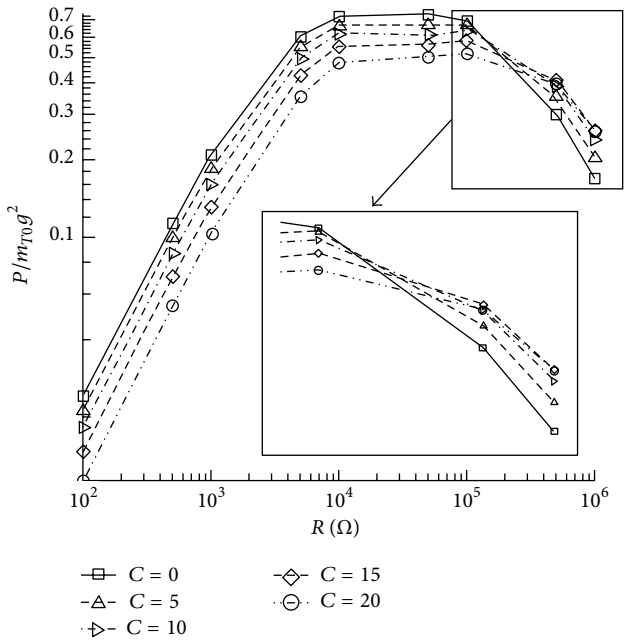

Figure 15: Tapering and electric resistance effects on bimorph with parallel connection.

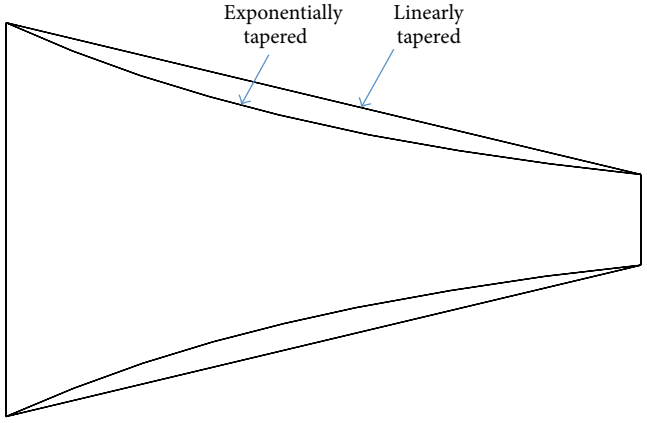

Figure 16: Exponentially ($c = 28.92$) and linearly tapered energy harvesters with the same base and tip (b_T) widths.

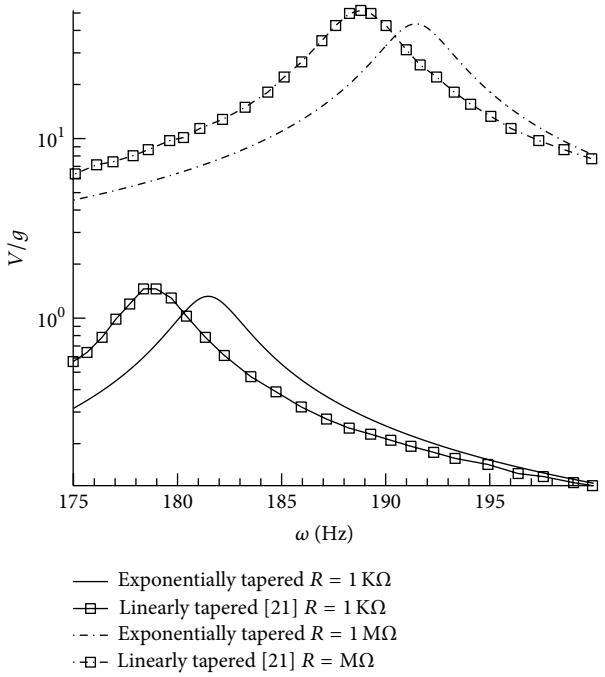

Figure 17: Comparison of V/g values between exponentially and linearly tapered energy harvesters.

Table 4: Energy harvesters modelling parameters.

Parameter	Value
L (mm)	50.8
b_0 (mm)	31.5
b_T (mm)	7.25
h_s (mm)	0.14
h_p (mm)	0.26
M_t (gr)	0.0164
z	0.0073

results of the given analytical solution with experimental and numerical method results proves the analytical formulation validity to calculate the generated voltage. After verifying the formulations, parametric study is performed on tapering parameter, beam's length, and electric resistance. While tapering the beam, its first natural frequency increases, therefore two approaches, that is, using a thinner substrate layer or mounting a tip mass, have been implemented to adjust its natural frequency. In both methods, tapering leads to a maximum value for the voltage density for different lengths of the beam. It has been also noted that electric resistance is an effective parameter on the output power of the piezoelectric beam. Our study has shown that the efficacy of tapering depends on the electric resistance, where in lower values of electric resistance than a specified one the tapering reduces the electric power density. Consequently, not only does the electric power generated in energy harvesting device depend on tapering, but also it is dependent on all parameters such as beam's length, thickness, tip mass, and electric resistance. Therefore, it is feasible to improve the power density of the piezoelectric beam by tapering it exponentially provided that all parameters are considered in designing procedure.

Conflict of Interests

The authors declare that there is no conflict of interests regarding the publication of this paper.

Acknowledgments

The experiments were conducted at Mechanics of Smart Materials (MSM) Lab. and Modal Analysis Lab., Aerospace Engineering Department, Sharif University of Technology.

References

[1] C. B. Williams and R. B. Yates, "Analysis of a micro-electric generator for microsystems," *Sensors and Actuators A: Physical*, vol. 52, no. 1–3, pp. 8–11, 1996.

[2] S. Priya and D. J. Inman, *Energy Harvesting Technologies*, Springer, Boston, Mass, USA, 2009.

[3] D. Guyomar, A. Badel, E. Lefeuvre, and C. Richard, "Toward energy harvesting using active materials and conversion improvement by nonlinear processing," *IEEE Transactions on Ultrasonics, Ferroelectrics, and Frequency Control*, vol. 52, no. 4, pp. 584–594, 2005.

[4] N. E. Dutoit, B. L. Wardle, and S.-G. Kim, "Design considerations for mems-scale piezoelectric mechanical vibration energy harvesters," *Integrated Ferroelectrics*, vol. 71, no. 1, pp. 121–160, 2005.

[5] A. Erturk and D. J. Inman, "On mechanical modeling of cantilevered piezoelectric vibration energy harvesters," *Journal of Intelligent Material Systems and Structures*, vol. 19, no. 11, pp. 1311–1325, 2008.

[6] G.-Q. Wang and Y.-M. Lu, "An improved lumped parameter model for a piezoelectric energy harvester in transverse vibration," *Shock and Vibration*, vol. 2014, Article ID 935298, 12 pages, 2014.

[7] H. A. Sodano, G. Park, and D. J. Inman, "Estimation of electric charge output for piezoelectric energy harvesting," *Strain*, vol. 40, no. 2, pp. 49–58, 2004.

[8] A. Erturk and D. J. Inman, "A distributed parameter electromechanical model for cantilevered piezoelectric energy harvesters," *Journal of Vibration and Acoustics*, vol. 130, no. 4, Article ID 041002, 2008.

[9] A. Erturk and D. J. Inman, "An experimentally validated bimorph cantilever model for piezoelectric energy harvesting from base excitations," *Smart Materials and Structures*, vol. 18, no. 2, Article ID 025009, 2009.

[10] L. Mateu and F. Moll, "Optimum piezoelectric bending beam structures for energy harvesting using shoe inserts," *Journal of Intelligent Material Systems and Structures*, vol. 16, no. 10, pp. 835–845, 2005.

[11] J. Baker, S. Roundy, and P. Wright, "Alternative geometries for increasing power density in vibration energy scavenging for wireless sensor networks," in *Proceedings of the 3rd International Energy Conversion Engineering Conference*, pp. 959–970, August 2005.

[12] S. Lee, B. D. Youn, and B. C. Jung, "Robust segment-type energy harvester and its application to a wireless sensor," *Smart Materials and Structures*, vol. 18, no. 9, Article ID 095021, 2009.

[13] D. Benasciutti, L. Moro, S. Zelenika, and E. Brusa, "Vibration energy scavenging via piezoelectric bimorphs of optimized shapes," *Microsystem Technologies*, vol. 16, no. 5, pp. 657–668, 2010.

[14] M. Defosseux, M. Allain, and S. Basrour, "Comparison of different beam shapes for piezoelectric vibration energy harvesting," in *Proceedings of the International Conference on Micro and Nanotechnology for Power Generation and Energy Conversion Applications (PowerMEMS '10)*, Leuven, Belgium, 2010.

[15] J. Park, S. Lee, and B. M. Kwak, "Design optimization of piezoelectric energy harvester subject to tip excitation," *Journal of Mechanical Science and Technology*, vol. 26, no. 1, pp. 137–143, 2012.

[16] S. P. Matova, M. Renaud, M. Jambunathan, M. Goedbloed, and R. Van Schaijk, "Effect of length/width ratio of tapered beams on the performance of piezoelectric energy harvesters," *Smart Materials and Structures*, vol. 22, no. 7, Article ID 075015, 2013.

[17] M. Gallina and D. Benasciutti, "Finite element analysis of optimized piezoelectric bimorphs for vibrational 'energy harvesting,'" in *Proceedings of the International CAE Conference*, pp. 1–4, Verona, Italy, 2013.

[18] Q. C. Guan, B. Ju, J. W. Xu, Y. B. Liu, and Z. H. Feng, "Improved strain distribution of cantilever piezoelectric energy harvesting devices using H-shaped proof masses," *Journal of Intelligent Material Systems and Structures*, vol. 24, no. 9, pp. 1059–1066, 2013.

[19] F. Goldschmidtboeing and P. Woias, "Characterization of different beam shapes for piezoelectric energy harvesting," *Journal of Micromechanics and Microengineering*, vol. 18, no. 10, Article ID 104013, 2008.

[20] J. M. Dietl and E. Garcia, "Beam shape optimization for power harvesting," *Journal of Intelligent Material Systems and Structures*, vol. 21, no. 6, pp. 633–646, 2010.

[21] M. Rosa and C. de Marqui Jr., "Modeling and analysis of a piezoelectric energy harvester with varying cross-sectional area," *Shock and Vibration*, vol. 2014, Article ID 930503, 9 pages, 2014.

[22] S. Paquin and Y. St-Amant, "Improving the performance of a piezoelectric energy harvester using a variable thickness beam," *Smart Materials and Structures*, vol. 19, no. 10, Article ID 105020, 2010.

[23] S. Ben Ayed, A. Abdelkefi, F. Najar, and M. R. Hajj, "Design and performance of variable-shaped piezoelectric energy harvesters," *Journal of Intelligent Material Systems and Structures*, vol. 25, no. 2, pp. 174–186, 2014.

[24] C. Y. Wang and C. M. Wang, "Exact vibration solution for exponentially tapered cantilever with tip mass," *Journal of Vibration and Acoustics, Transactions of the ASME*, vol. 134, no. 4, Article ID 041012, 2012.

[25] L. Meirovitch, *Fundamentals of Vibrations*, McGraw-Hill Higher Education, 2001.